Research Article

Ahmed B. Khoshaim, Essam B. Moustafa*, and Rasha A. Youness

Antibacterial, mechanical, and dielectric properties of hydroxyapatite cordierite/zirconia porous nanocomposites for use in bone tissue engineering applications

https://doi.org/10.1515/ntrev-2023-0175
received September 9, 2023; accepted November 28, 2023

Abstract: We made nanocomposites with different amounts of hydroxyapatite (HA), cordierite (Cord), and zirconia (ZrO_2), then sinterized them and studied them using X-ray diffraction (XRD) technique and field emission scanning electron microscopy (FESEM). Additionally, the bioactivity of the sintered samples was assessed in vitro following treatment with simulated bodily fluid (SBF), and FESEM was used to validate the creation of the HA layer on their surfaces. Measurements were also made for mechanical and antibacterial properties. All materials' electrical and dielectric characteristics were assessed before and after being treated with SBF solution. All of the samples that were studies had porosity increases of about 7.14, 22.44, 43.87, and 73.46%. This was because the sintering temperature was lowered while the concentration of ZrO_2 in the samples increased. Also, the microhardness got 5.35, 14.28, 28.57, and 55.35% better because there was more ZrO2 and Cord in the samples than in the sample that did not have them. In addition, the compressive strength of all studied samples followed this trend, as it increased by 2.81, 7.79, 17.74, and 34.32% due to the reasons mentioned above. Furthermore, the electrical conductivity of the tested samples decreased as they increased their ZrO_2 and Cord contents. The bioactivity of the research materials also somewhat decreased as the concentrations of Cord and ZrO_2 were enhanced over time. Due to the magnesium (Mg^{2+}) ions found in Cord's composition and the samples' porousness, which aided in forming an apatite layer on their surface, their bioactivity behavior was slightly reduced. All the samples that were looked at had a strong antibacterial effect on *Staphylococcus epidermidis* (*S. epidermidis bacteria*), which stopped their growth to a point between 2.33–3.30 mm. These results supported the notion that the generated porous nanocomposites have great potential for use in bone tissue engineering.

Keywords: porous nanocomposites, osseointegration, antibacterial effect, mechanical properties, bone tissue engineering applications

1 Introduction

Focusing on biomaterials used in the treatment of bone tissue, much effort has recently been put into designing biomaterials for repairing injured human tissues. It should be noted that these endeavors do not end due to the wide variety of standards for materials used in orthopedic applications, which are strongly affected by industrial progress [1–5]. Unfortunately, bone resorption, partly caused by wear and corrosion debris from the implants infiltrating the surrounding tissue and causing the implants to become loose, necessitates the replacement of 10–20% of implanted joints within 15–20 years. A superb biomaterial for surgical implantation should thus have a good combination of various physical properties. It should, first and foremost, be highly wear and corrosion resistant and also have good biocompatibility. Second, a material with a low modulus and high strength closer to the bone will be preferred. The material surface must maintain its integrity under pressure as the third important component [6]. Based on this, the best candidate materials should possess several properties such as osteoconductivity, biocompatibility, antimicrobial, electrical, and mechanical properties. Since no single material can satisfy all these needs, scientists have created composite materials to meet these diverse requirements [7,8].

*** Corresponding author: Essam B. Moustafa,** Mechanical Engineering Department, Faculty of Engineering, King Abdulaziz University, P.O. Box 80204, Jeddah, Saudi Arabia, e-mail: abmostafa@kau.edu.sa
Ahmed B. Khoshaim: Mechanical Engineering Department, Faculty of Engineering, King Abdulaziz University, P.O. Box 80204, Jeddah, Saudi Arabia
Rasha A. Youness: Spectroscopy Department, National Research Centre, El Buhouth St., Dokki, 12622 Giza, Egypt

HA ($Ca_{10}(PO_4)_6(OH)_2$) is one of the materials with the best prospects for use in orthopedic and dental applications. Its biocompatibility and capacity for bone bonding account for this remarkable significance in these various biological applications. In addition, the formation of B–type carbonated hydroxyapatite (B–CHA), which gives HA more desirable qualities, is the consequence of the partial replacement of certain phosphate (PO_4^{3-}) groups in its crystal structure by carbonate (PO_3^{2-}) groups [9]. Another important element in improving CHA's biological importance is its preparation in the nanometer range, which allows for stronger interactions with proteins and osteoblastic cells [10]. However, its weak mechanical qualities limit its potential for use in biomedicine. The composites' preparation or morphology can be changed to enhance HA's mechanical properties [11–13].

Aluminum oxide (Al_2O_3), and MgO, make up the ternary system of oxide that makes up Cord ($Mg_2Al_4Si_5O_{18}$) [14]. Due to its hardness, resistance to compression, chemical inertness, and porosity, which are suitable for the majority of the requirements for the success of biological materials, Cord has demonstrated remarkable success in various manufacturing methods in a variety of applications, particularly those involving biology [15].

One of the most often used biomaterials is ZrO_2 because of its promising properties, which include remarkable mechanical and thermal capabilities. As the color is so remarkably similar to the color of teeth, it also offers great aesthetic attributes. Because of these positive characteristics, it was initially used in dentistry in the 1990s [16,17]. As ZrO_2 is a chemical oxide, it also has the advantage of not dissolving in water, which lowers bacterial adhesion and exhibits minimum cytotoxicity. Moreover, it offers excellent corrosion resistance. The characteristics mentioned earlier have led to an expansion of the biological applications of ZrO_2 to orthopedic applications. Nevertheless, ZrO_2's fundamental drawback limiting its clinical application is that it is bioinert [18]. As a result, creating nanocomposites with bioactive phases is one of the most promising ways to solve this issue.

The incidence of biomaterial-centered illnesses is one of the main disadvantages of using biomaterials. The host will interact with the biomaterial after implantation by developing a conditioning coating on its surface. The surface characteristics of the biomaterial mediate microorganism adhesion. The infection will begin when microorganisms on the surface start to multiply. For example, according to an *in vitro* investigation, *Staphylococcus epidermidis* multiplied in the first 8–12 h following implantation. Efforts have been made to avoid microbial contamination of foreign materials during implantation. Antibiotic usage undoubtedly helps limit the frequency of infections focused on biomaterials, but a sizable proportion of patients struggle with this illness [19].

The effect of ZrO_2 on enhancing HA's mechanical and antibacterial properties has been studied by many researchers [20–23]. However, according to the authors' knowledge, the effect of adding different contents of Cord on HA has not gained the attention of researchers before. Therefore, one might expect that the combination of adding these two reinforcements, *i.e.*, ZrO_2 and Cord, to HA and studying the biological, physical, mechanical, electrical, and dielectric properties of the resulting nanocomposites has not been studied. In addition, the novelty of this study extends to the investigation of the electrical and dielectric properties of samples after soaking them in simulated body fluid (SBF) for 10 days.

2 Materials and methods

2.1 Preparation of CHA nanopowders

To physically activate the chemical interaction between calcium carbonate ($CaCO_3$) and calcium hydrogen phosphate dihydrate ($CaHPO_4{\cdot}2H_2O$) powders as reported in the studies by Youness *et al.* [24,25], CHA nanopowders have been created in this study with the use of a high-energy ball mill (HEBM). In a nutshell, HEBM was combined with $CaHPO_4{\cdot}2H_2O$ and $CaCO_3$ for 5 h while rotating at 150 rpm. After that, milling was carried out for 10 h in dry conditions using 10 mm-diameter alumina balls and a 10:1 ball-to-powder ratio (BPR). The obtained CHA nanopowders phase composition, particle size, and crystallinity were investigated by XRD technique (Philips PW 1373; diffractometer with CuK–Ni filtered radiation at a scan speed of 0.5 min^{-1}) and high-resolution transmission electron microscopy–selected area electron diffraction (HRTEM-SAED; JEOL JEM-2100 Japan, operated at accelerating voltage of 120 kV).

2.2 Preparation of Cord nanopowders

Al_2O_3 (98.5%), SiO_2 (97.5%), and MgO (98%) powder were used to create the first combination of the Cord stoichiometric composition ($2MgO{\cdot}2Al_2O_3{\cdot}5SiO_2$). The powder was mechanically blended for 30 min to verify the homogeneity of the representative batch. This mixture was dried and then heated for 3 h at 1,300°C with air present to study the reaction process. Then, the

resultant Cord powders were investigated using XRD and HRTEM-SAED techniques.

2.3 Fabrication of HA/Cord/ZrO_2 nanocomposites

The purchased ZrO_2 powders (purity 99.5%) were mixed with the as-prepared materials, *i.e*., CHA and Cord, using HEBM for 20 h and BPR = 5:1 running in the dry condition in alumina vials and balls with diameters of 10 mm at 150 rpm as a rotational speed. Then, the nanocomposite powders were pressed using a hydraulic press at 30 MPa and sintered at 600°C for 1 h at a heating rate of 5°C/min. The compositions of the samples prepared and their abbreviations are presented in Table 1.

2.4 Investigation of phase composition and microstructure of the sintered nanocomposites

With the XRD method's assistance, the sintered nanocomposites' phase composition was examined. In addition, FESEM (Philips XL3000 type) was used to analyze the microstructure of the sintered nanocomposites.

2.5 Biological properties of the tested samples

2.5.1 *In vitro* bioactivity assessment

It was possible to assess the *in vitro* bioactivity of the materials by letting the created nanocomposites soak in an SBF prepared in accordance with the guidelines provided by Kokubo *et al*. [26,27] for 10 days while maintaining the ratio of glass grains to the volume of solution = 0.01g/ml [28]. FESEM was then used on the soaked samples to look into the changes to their surfaces brought on by soaking them in SBF solution.

Table 1: Scheme of the prepared nanocomposites referring to the sample code and its composition (vol%)

Samples code	HA	Cord	ZrO_2
CZ0	100	0	0
CZ1	97	2.5	0.5
CZ2	94	5	1
CZ3	88	10	2
CZ4	76	20	4

2.5.2 Antibacterial effect

The disc–diffusion method was used in the current study to assess the antibacterial activity of sintered nanocomposites against *S. epidermidis* and *Escherichia coli*, two typical species of Gram-positive and Gram-negative bacteria, respectively.

2.6 Measurement of the different properties of the obtained nanocomposites

2.6.1 Physical properties

We sintered all the samples at 600 °C for one hour and used the Archimedes method (ASTM B962-13), which is explained in Ref. [29], to figure out their bulk density and apparent porosity.

2.6.2 Mechanical properties

The microhardness of the sintered samples was determined in accordance with ASTM: B933-09, as mentioned in our most recent papers [30,31]. Notably, each data point included measurements of at least five indentations per specimen. On the other hand, all samples underwent the compressive strength test under ASTM E9.

2.6.3 Electrical and dielectric properties

Using a broadband dielectric spectroscopic method, the produced samples' AC electrical conductivity, dielectric constant, and dielectric loss were assessed at room temperature before and after soaking in the SBF solution for 10 days.

3 Results and discussion

3.1 Investigation of the phase composition, crystallinity, and particle size of the starting materials

XRD equipment was used to investigate the phase composition of all starting materials, such as HA, Cord, and ZrO_2. The results are shown in Figure 1. By analyzing the obtained data, it is possible to see the clarity of distinct HA

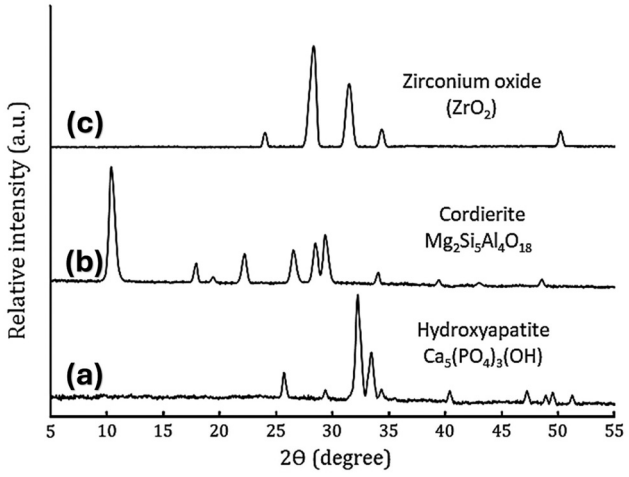

Figure 1: XRD patterns of the as-prepared powders, *i.e.*, (a) HA, (b) Cord, and (c) ZrO_2 powders.

XRD peaks without the presence of any other XRD peaks. This result suggests that the HA was produced correctly. The original materials, such as HA, Cord, and ZrO_2, may also be found to be in the nanoscale range based on the observed broadness in their diffraction peaks. One of the most important advantages of nanostructured biomaterial is its improved capacity to interact with proteins and cells that make bone [32].

The particle sizes and crystallinity of the HA, Cord, and ZrO2 powders used are shown in Figure 2(a)–(c). The pictures in these figures make it very clear that the HA, Cord, and ZrO_2 are made up of spherical nanoparticles. This is because the milling process seems to have strongly grouped the HA powder particles together.

It is important to remember that the average particle sizes of HA, Cord, and ZrO_2 are 42.34, 56.62, and 77.74 nm, respectively. In addition, the SAED patterns demonstrated the presence of polycrystalline diffraction rings generated from the *d*-spacing ICCD file cards previously described.

3.2 Characterization of the sintered nanocomposites

3.2.1 XRD analysis

The XRD patterns of each sintered sample are displayed in Figure 3. The following key facts are supported by this figure and can be distilled as follows:

- The typical XRD peaks for HA, Cord, and ZrO2 are clearly visible.
- Despite being treated to a high sintering temperature, there is no evidence that the HA particles decompose and form β-tricalcium phosphate (β-TCP; $Ca_3(PO_4)_2$).
- No other peaks could be detected on the X-ray diffractogram, indicating that the component phases of these nanocomposites did not interact and that there was no contamination during the synthesis of the nanocomposites or the sintering process.
- The sintering process, which reflects improved crystallization, shows a noticeable sharpness at all peaks compared to Figure 1.

3.2.2 Investigation of the microstructure of the samples by FESEM

The microstructure of all fabricated samples was analyzed using FESEM, as shown in Figure 4(a)–(e). From this figure, one can observe the porous structure of all samples. The reason for obtaining a porous structure for all the samples prepared from the initial sample, *i.e.*, CZ0, to the last sample, *i.e.*, CZ4, is the high melting temperatures of HA (1,650°C), Cord (1,460°C), and ZrO_2 (2,715°C) compared to the temperature used to perform the sintering process (600°C). As discussed earlier, since ZrO_2 has the highest melting temperature among the other materials used to prepare nanocomposites, increasing its volume percent is considered a major factor in increasing the porosity level. This conclusion is based on the significant increase in the number of pores and the proportion of ZrO_2. Another explanation for the observed increase in porosity as a result of increasing the content of ZrO_2 is the difference in particle sizes between HA (42 nm) and ZrO_2 (77 nm), as discussed in Section 3.1, which led to more pores between their particles due to a reduction in the contact area between HA and ZrO_2 particles, which resulted in hollow areas [33].

3.3 Biological properties of the tested samples

3.3.1 *In vitro* bioactivity assessment

In general, treatment in an SBF solution is known as a straightforward and affordable test to reliably assess a biomaterial's capacity to create a bone-like layer on its surface following immersion in it. It should be noted that

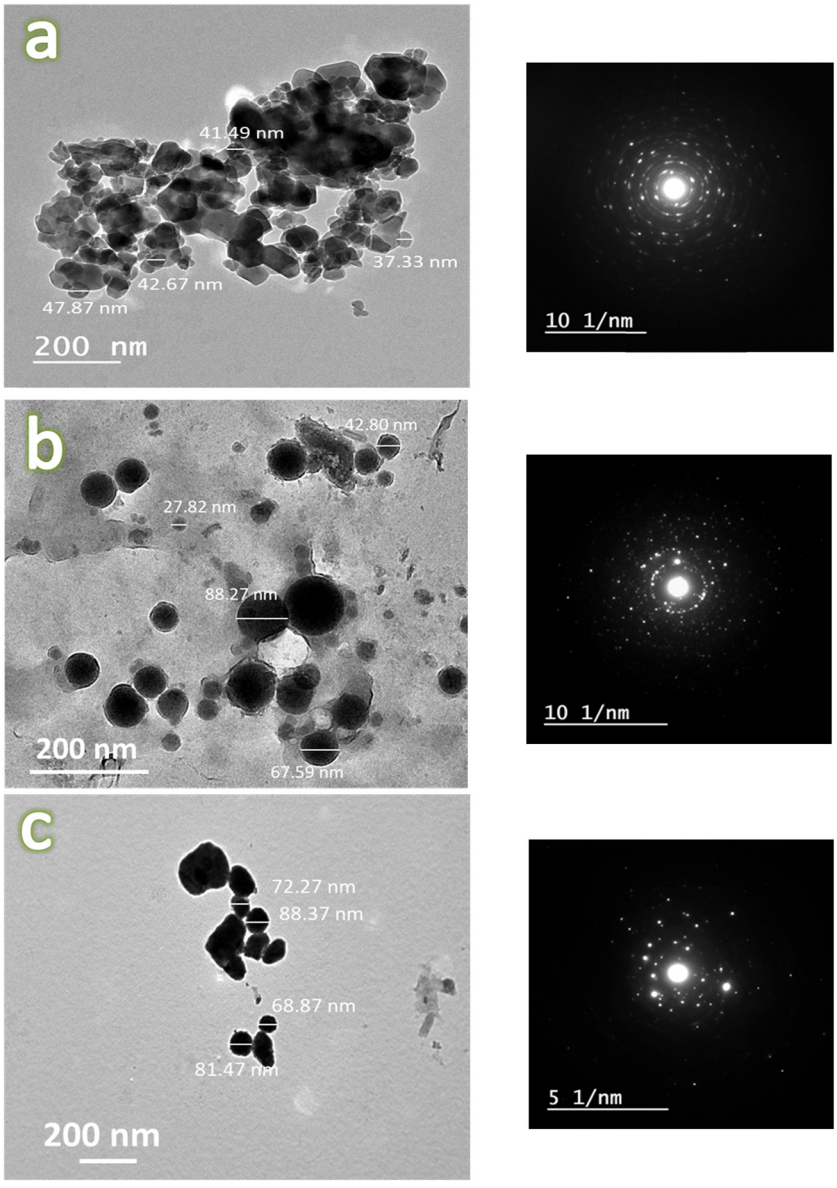

Figure 2: HRTEM images and their corresponding SAED patterns for the starting materials, *i.e.*, (a) HA, (b) Cord, and (c) ZrO_2 powders.

the "bioactivity property" refers to a substance's capacity to build the desired layer. Based on this, the substance is thought to exhibit superb adhesion to nearby living bone tissue when it is transplanted into a person [34]. The sintered samples, *i.e.*, CZ0, CZ2, and CZ4, were incubated in the SBF solution for 10 days, and then they were submitted to FESEM to provide the reader with visual proof of the creation of the HA layer on their surfaces shown in Figure 5(a)–(c). Given that the bioactivity of the sintered nanocomposites displays a falling sequence, CZ0 > CZ2 > CZ4, it is clear that all sintered samples have shown a good formation for the apatite layer on their surfaces. In other words, when Cord and ZrO_2 concentrations rise, but HA amounts fall, the investigated samples' bioactivity marginally declines. This observation is supported by the generated layer almost completely covering the CZ0 sample's surface. On the other hand, this layer gradually thins down as Cord and ZrO_2 levels rise, thankfully without significantly affecting the samples' bioactivity. The obtained results can be explained in terms of many factors. First, the presence of negative charge content of HA, namely, $(PO_4)^{3-}$, which may quickly absorb the cations, specifically calcium $(Ca)^{2+}$, present in the solution and result in the creation of an amorphous calcium phosphate layer, as indicated in our previous study [35]. The generated layer is then crystallized on the sample surface to produce HA crystals. Second, the Mg^{2+} ions in the Cord composition

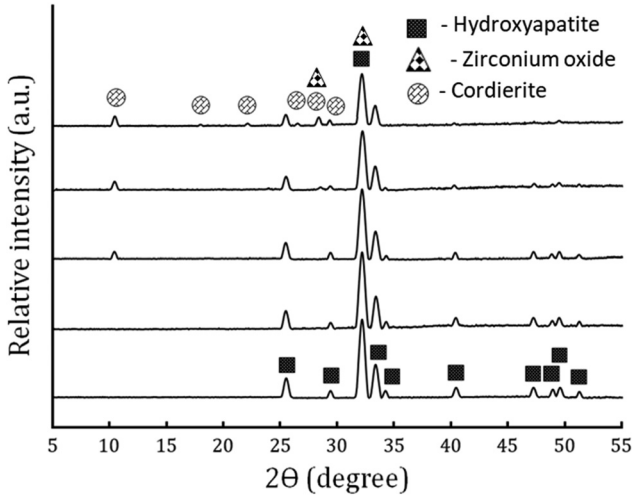

Figure 3: XRD patterns of sintered HA/Cord/ZrO_2 nanocomposites samples.

encouraged the growth of apatite on the sample surface [36]. Third, an increase in sample porosity encourages the development of apatite on a sample's surface. This is because materials with larger porosities will have better SBF flow, which will provide simpler ion dissolution between samples and SBF solution [37]. Noteworthy, the literature highly supports the obtained results [38,39]. Based on the findings, it is possible to restore injured tissues, such as the hip, knee, teeth, and joints, using the nanocomposites that have been created [40].

3.3.2 Antibacterial effect

In most cases, bacterial infections acquired during surgical procedures cause severe difficulties following the implantation of biomaterials into people [41]. Based on this reality, assessing a possible biomaterial's antibacterial performance is crucial. Therefore, using disc diffusion tests, the antibacterial properties of the sintered samples were examined against *S. epidermidis* (ATCC12228) and *E. coli* (ATCC25922), which are Gram+ and Gram– bacteria, respectively. The results are displayed in Figure 6(a) and (b), and the measured diameter of the inhibition zones is tabulated in Table 2. The acquired images show that the growth of *E. coli* was markedly inhibited in all tested samples, including Cord and ZrO_2-free samples. These results can be attributed to the strong antibacterial effects of ZrO_2 and MgO present in the Cord and possible changes in the pH value due to the possible dissolution of the CZ0 sample in the surrounding medium. It is important to remember that these

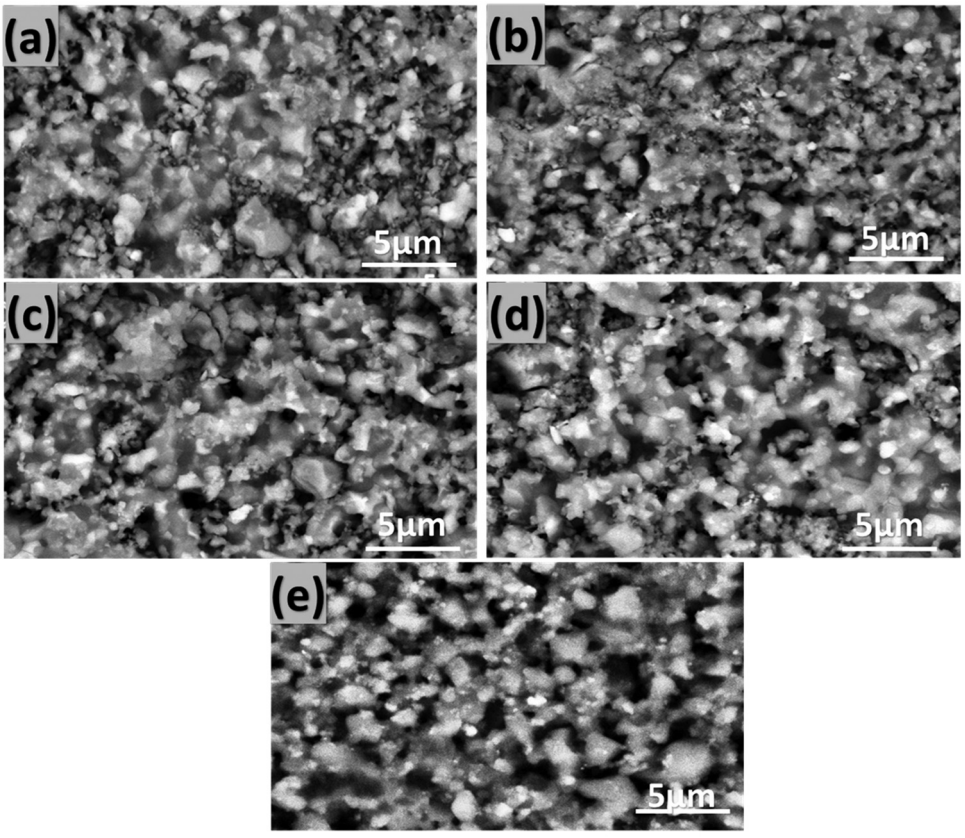

Figure 4: FESEM micrographs of all sintered samples; namely (a) CZ0, (b) CZ1, (c) CZ2, (d) CZ3, and (e) CZ4.

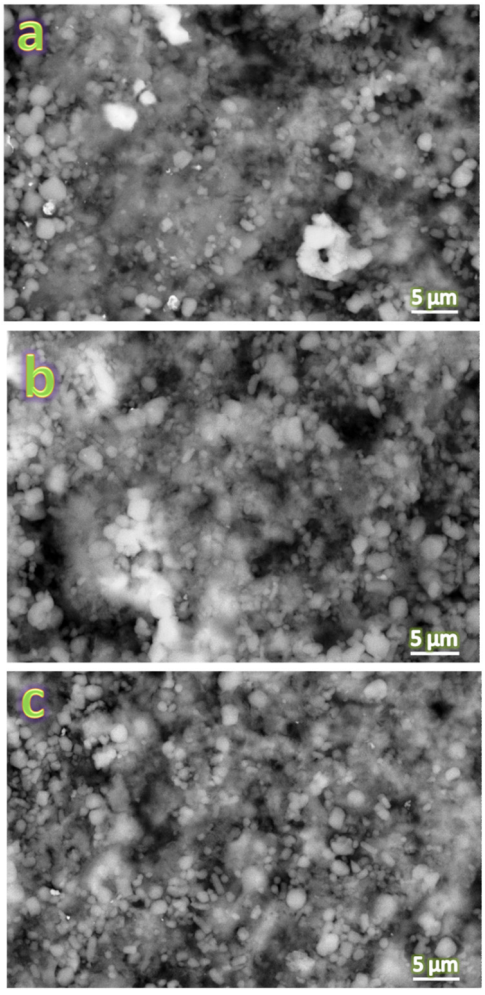

Figure 5: FESEM micrographs of (a) CZ0-, (b) CZ2-, and (c) CZ4-sintered samples after their treatment in the SBF solution for 10 days.

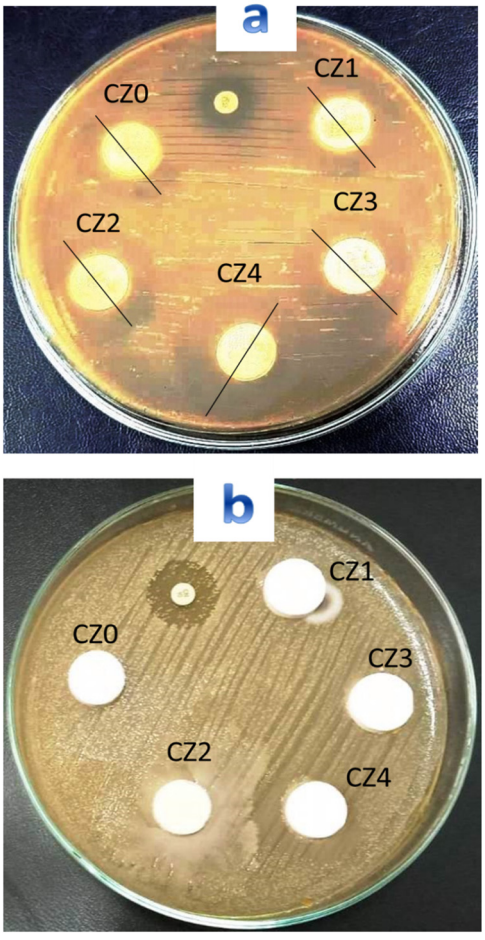

Figure 6: Photos of Petri dishes after conducting agar disc–diffusion assays against (a) *S. epidermidis* and (b) *E. coli* for sintered samples.

nanocomposites do not affect the growth of *S. epidermidis*. Here, we summarize how nano-ZrO_2 and nano-MgO in Cord kill bacteria.

Nano-ZrO_2 particles harm bacterial cell membranes by releasing active oxygen. As a result of this disruption, the cytoplasmic regions of the cells degrade, which also raises permeability [42]. On the other hand, the different possible antibacterial effects of MgO nanoparticles can be attributed to the fact that, according to references [43–45], the effects of MgO nanoparticles can be attributed to reactive oxygen species (ROS) production preventing *E. coli* from growing. The capacity of MgO to attach to the cell membrane and induce damage, resulting in an observable change in the shape of the cell membrane and causing deformation and cell death, is another antibacterial mechanism for Gram-negative bacteria. Gram-positive bacteria, on the other hand, have a strong peptidoglycan protective coating; therefore, this method does not apply to them.

Table 2: The measured inhibition zone diameters for all examined nanocomposites samples against *S. epidermidis* and *E. coli* bacteria

Samples' code	Inhibition zone (mm)	
	S. epidermidis	*E. coli*
CZ0	2.33	...
CZ1	2.50	...
CZ2	2.78	...
CZ3	3	...
CZ4	3.3	...

3.4 Measurement of the different properties of the obtained nanocomposites

3.4.1 Physical properties

All samples' bulk density and apparent porosity are depicted in Figure 7(a) and (b), respectively. The findings show that

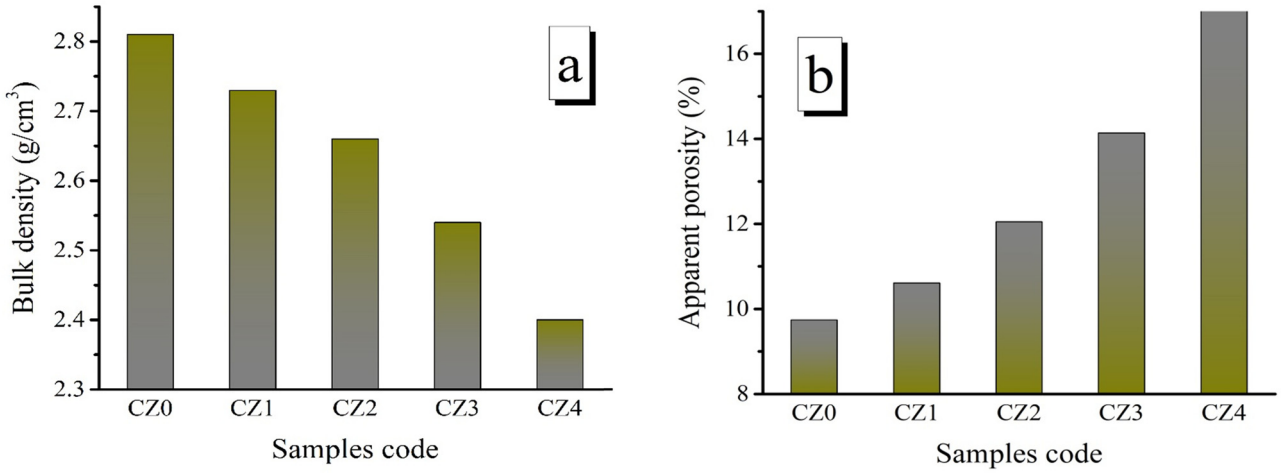

Figure 7: (a) Bulk density and porosity and (b) relative density of samples sintered at 600°C for 1 h.

the bulk density of the samples under investigation noticeably decreased when the volume percentages of Cord and ZrO_2 were successively increased. It is interesting to note that this decrease is not significant because HA (3.15 g/cm^3) was substituted with a lighter material, namely, Cord (2.28 g/cm^3), and a heavier material, namely, ZrO_2 (5.68 g/cm^3), while percentage increases for ZrO_2 were only 4 and Cord 20 vol%, respectively. In contrast, as discussed in Section 3.2.2, the low temperature used in the sintering process and the presence of ZrO_2 with a higher melting temperature, *i.e.*, 2,715°C, contributed to the increased porosity of the sintered samples.

These findings are well aligned with those covered in Section 3.2.2. Various variables greatly influence ceramic materials' densification, including the sintering temperature, the surrounding environment, and the initial powder's grain size. Most notably, it can be assumed that if the materials utilized are in the small size range, the porosity of the generated composites will be higher since nano-sized powders exhibit superior condensation behavior than micron-sized ones at lower sintering temperatures [46].

3.4.2 Mechanical properties

The microhardness and compressive strength measurements for all nanocomposites are shown in Figure 8(a) and (b). These figures demonstrate how the combined effects of Cord and ZrO_2 boosted all the tested mechanical qualities. CZ0, CZ1, CZ2, CZ3, and CZ4 samples' microhardness values are 2.80, 2.95,

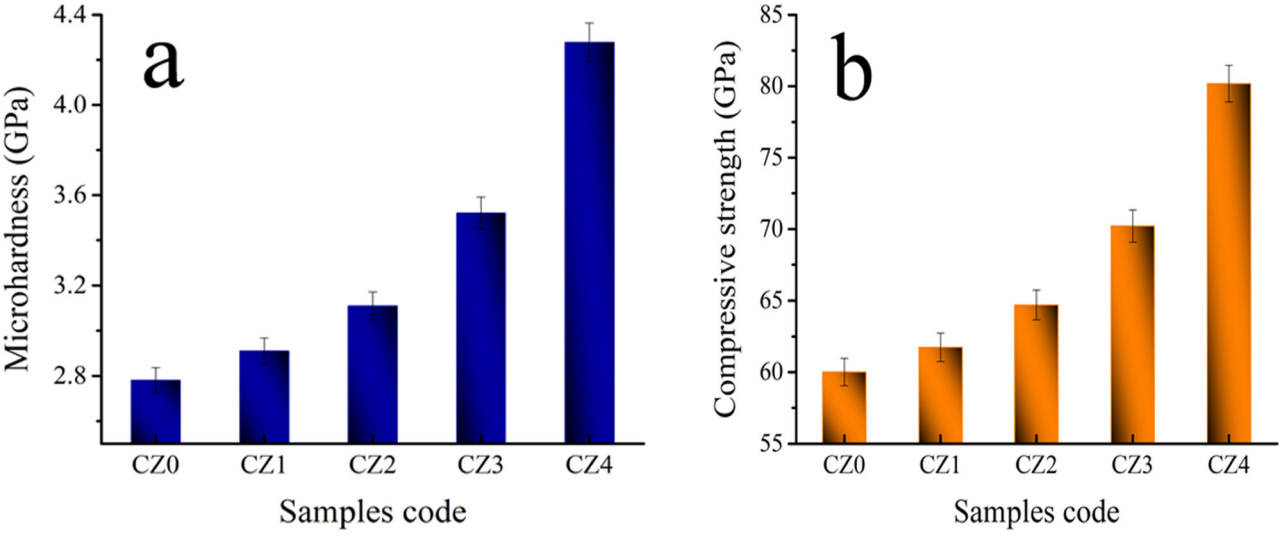

Figure 8: (a) Microhardness and (b) compressive strength of samples sintered at 600°C for 1 h.

3.20, 3.60, and 4.35 Hv, respectively, whereas their compressive strength values are 60.30, 62, 65, 71, and 81 MPa, respectively. Better mechanical properties of the reinforcements used in this study, *i.e.*, Cord and ZrO_2, can be used to explain the results obtained. These outcomes are quite consistent with those mentioned in Abushanab *et al.* [47]. It is important to note that the CZ4 sample's compressive strength is close to that of cortical bone (100–150 MPa), indicating that the surrounding bone would not experience the stress-shielding effect if the CZ4 sample was implanted into human bone. Importantly, the stress-shielding effect is extremely damaging and causes a major weakening of the bone since it lacks the stimuli required for the ongoing remodeling process, according to Wolff's law [48].

Table 4: ε′ and ε″ of all examined samples measured at different frequencies, i.e., 1, 5, 10, and 20 MHz

	1 MHz	5 MHz	10 MHz	20 MHz
			ε′	
CZ0	4.911	3.401	1.991	1.477
CZ1	5.977	4.398	2.511	1.741
CZ2	7.700	6.072	3.362	2.228
CZ3	10.908	8.385	4.837	3.130
CZ4	14.548	11.929	7.829	4.351
			ε″	
CZ0	1.112	8.991	7.011	5.101
CZ1	0.136	0.132	0.099	0.078
CZ2	0.177	0.169	0.146	0.124
CZ3	0.264	0.256	0.232	0.194
CZ4	0.397	0.392	0.364	0.291

3.4.3 Electrical and dielectric properties

There is no denying that the good electrical properties of biomaterials greatly aid in encouraging bone formation [49]. This research examines the electrical and dielectric characteristics of sintered nanocomposites and the effect of the produced apatite layer on their surfaces. Readers interested in studying diverse biomaterial characteristics will find this article new due to its immense relevance. The electrical conductivity and dielectric properties, such as the dielectric constant and dielectric loss, were tested in this regard at various frequencies. Measurements at 1, 5, 10, and 20 MHz were made, and the results are displayed in Tables 3 and 4. It is clear that the materials' electrical conductivity significantly decreased when the amounts of Cord and ZrO_2 increased due to their electrical insulating behavior. However, this propensity increased a little bit with frequency increasing. Polarization typically confers HA's dielectric properties, which are known to significantly improve bone tissue regeneration. Interestingly, the ε' represents the real component of the dielectric, *i.e.*, and the ε'' represents the imaginary part.

The natural frequency of these ions is the same as the frequency used in the AC field, according to Arul *et al.* [50]. The conduction of nano-sized HA at lower frequencies is due to the mild oscillation of Ca^{2+}, PO_4^{3-}, and OH^- ions. These dipole moments oscillate, resulting in ε' changes with a lower frequency. However, according to other research, the presence of protons (H^+), oxide ions (O^{2-}), and lattice hydroxyl (OH^-) ions is all that is necessary for HA to conduct, with Ca^{2+} and PO_4^{3-} ions having no impact on the conductance of the substance [51,52]. Given that the AC conductivity is subject to the following relationship, the CZ0 sample exhibits a constant rise with the increasing frequency at high frequencies:

$$\sigma_{ac} = \sigma_{dc} + B_{\omega s}, \quad (1)$$

where σ_{dc} is the DC electrical conductivity, B is a constant, ω is the angular frequency, and s is an exponent [53].

The rise in AC conductivity with higher frequency is due to the separation of a complex set of ions along the c-axis of the HA crystal structure [50]. The AC conductivity continuously declines when the amounts of Cord and ZrO_2

Table 3: AC conductivity of all examined samples measured at different frequencies, *i.e.*, 1, 5, 10, and 20 MHz

	AC conductivity (S/cm)			
	1 MHz	5 MHz	10 MHz	20 MHz
CZ0	1.21×10^{-6}	3.31×10^{-6}	6.55×10^{-5}	1.35×10^{-4}
CZ1	9.71×10^{-7}	2.60×10^{-6}	5.24×10^{-5}	1.11×10^{-4}
CZ2	7.71×10^{-7}	1.77×10^{-6}	3.90×10^{-5}	9.30×10^{-5}
CZ3	5.29×10^{-7}	9.61×10^{-7}	1.92×10^{-5}	5.70×10^{-5}
CZ4	1.08×10^{-7}	4.42×10^{-7}	5.76×10^{-6}	1.05×10^{-5}

Table 5: AC conductivity of all samples examined at different frequencies after incubation in SBF solution for 10 days

	AC conductivity (S/cm)			
	1 MHz	5 MHz	10 MHz	20 MHz
CZ0	1.31×10^{-6}	3.61×10^{-6}	7.14×10^{-5}	1.44×10^{-4}
CZ1	1.11×10^{-6}	3.12×10^{-6}	6.12×10^{-5}	1.36×10^{-4}
CZ2	9.36×10^{-7}	7.12×10^{-6}	4.79×10^{-5}	1.18×10^{-4}
CZ3	6.44×10^{-7}	1.20×10^{-6}	2.47×10^{-5}	7.09×10^{-5}
CZ4	1.35×10^{-7}	5.53×10^{-7}	7.11×10^{-6}	1.32×10^{-5}

Table 6: ε′ and ε″ of all samples evaluated at various frequencies after a 10-day incubation period in SBF solution

	1 MHz	5 MHz	10 MHz	20 MHz
		ε′		
CZ0	4.549	3.224	1.883	1.297
CZ1	5.352	3.911	2.207	1.510
CZ2	6.769	5.429	2.874	1.879
CZ3	9.205	7.172	4.002	2.570
CZ4	11.788	10.150	6.194	3.724
		ε″		
CZ0	0.10	0.083	0.063	0.047
CZ1	0.123	0.120	0.084	0.064
CZ2	0.161	0.150	0.121	0.106
CZ3	0.228	0.211	0.191	0.149
CZ4	0.348	0.321	0.298	0.232

are increased because there are fewer charge carriers, which raises the nanocomposites' resistance [54,55].

After analyzing the data, it is evident that ε' rises with higher Cord and ZrO_2 levels while falling with higher applied frequency. Notably, the values drastically dropped with frequency up to 10 MHz, but the decline in values becomes less pronounced at 20 MHz. The fact that the tested samples' dipoles prefer to point in the direction of the applied electric field may be used to explain why the values of ε' decreased as frequency increased. In contrast, because of the slower relaxation of the highly oriented dipoles at lower frequencies, ε' records substantially greater values [50]. Conversely, a reduction in the number of dipoles that point in the direction of the AC field is brought on by increasing the concentrations of Cord and ZrO_2. With the

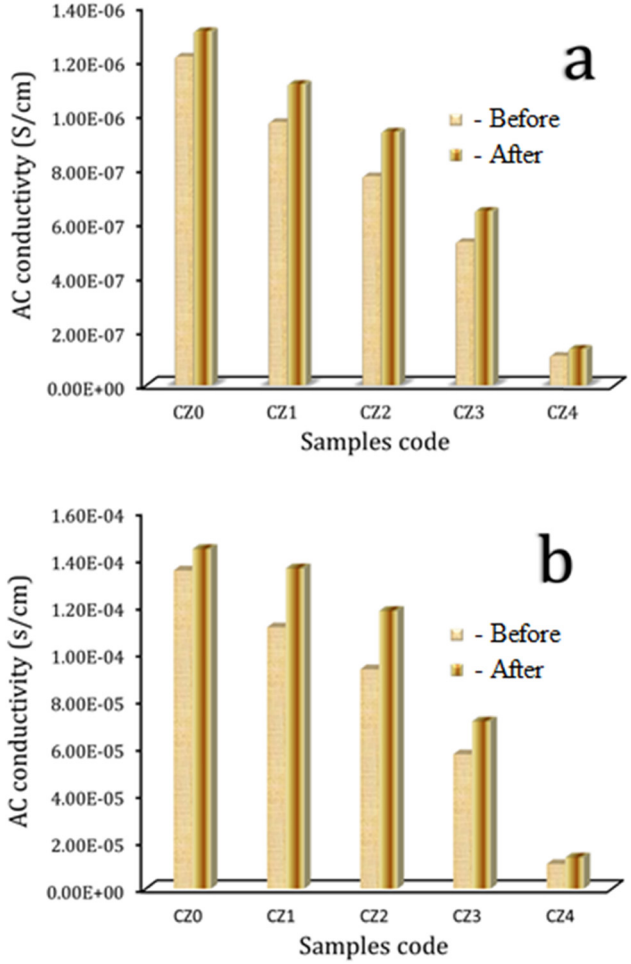

Figure 9: AC conductivity of all sintered samples before and after treatment in the SBF solution for 10 days at (a) 1 MHz and (b) 20 MHz.

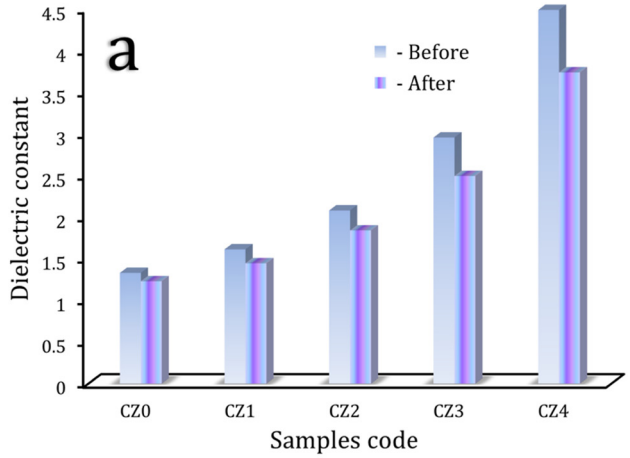

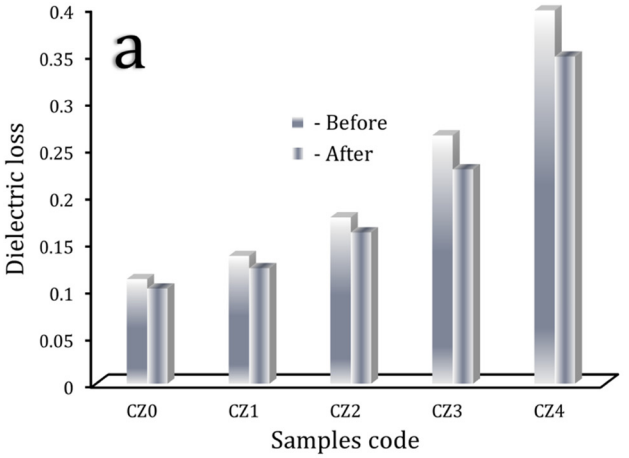

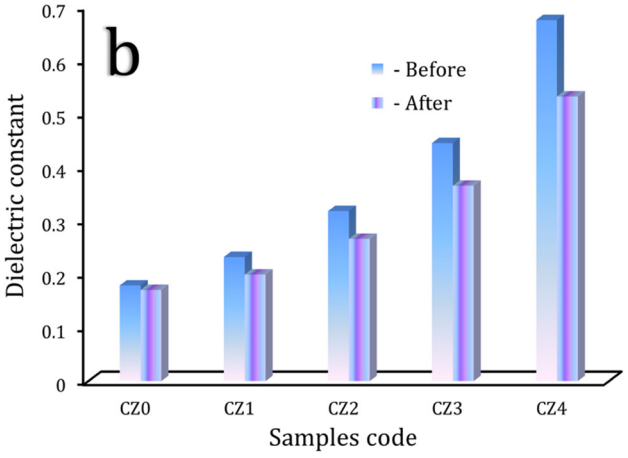

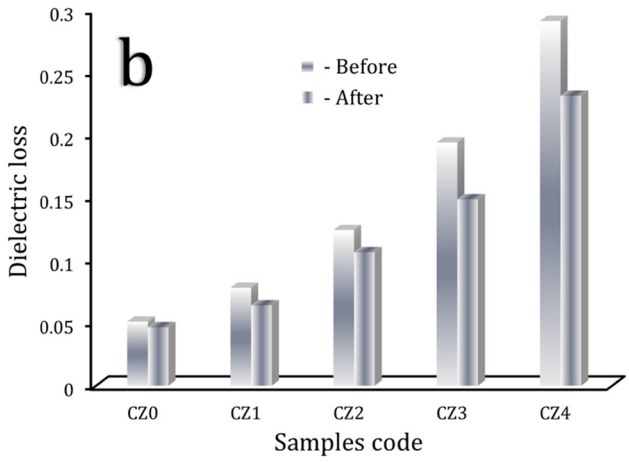

Figure 10: Dielectric constant of all sintered samples before and after treatment in the SBF solution for 10 days at (a) 1 MHz and (b) 20 MHz.

Figure 11: Dielectric loss of all sintered samples before and after treatment in the SBF solution for 10 days at (a) 1 MHz and (b) 20 MHz.

increasing frequency, a similar declining trend was also seen for ε''. The electric dipoles do not have enough time to align themselves with the applied electric field before it changes direction, which accounts for the apparent reduction caused by rising AC frequency; however, because there are fewer charge carriers, the higher contents of Cord and ZrO_2 aid in raising the measured ε'' values [56].

When the same frequencies were used, the AC electrical conductivity, ε', and ε'' were also measured to see what happened to the samples' electrical and dielectric behavior when a bone-like layer on the surface. The results were listed in Tables 5 and 6 as well. The characteristics of the nanocomposites indicated earlier before and after treatment in the SBF solution at lower and higher frequencies, *i.e.*, 1 and 20 MHz, are further depicted in Figures 9–11, respectively, to simplify the comparison of these properties before and after incubation in the SBF solution. The findings showed that the tested sample's AC conductance is very minimally increased by the produced HA layer. This favorable outcome can be due to reducing surface pores, which enhances conductivity. In addition, the insulating ceramic components present in the CZ1, CZ2, CZ3, and CZ4 samples are covered by this surface semiconductor layer. After incubation in the SBF solution, the values of ε' and ε'' displayed an opposite pattern, declining, which reflected the reduced dielectric characteristics of the examined samples.

4 Conclusions

In the present study, nanopowders of Cord, and HA have been successfully prepared with the help of high-energy ball mill and sintering process. Subsequently, different contents of Cord were added to HA in combination with ZrO_2 to produce nanocomposites with promising properties for use in bone tissue engineering applications. The findings demonstrated that there were porosity increases of around 7.14, 22.44, 43.87, and 73.46% in all of the studied samples.

This occurred as a result of the samples' increasing ZrO_2 concentration and decreasing sintering temperature. Furthermore, compared to the sample without ZrO_2 and Cord, the microhardness was enhanced as a result of the higher ZrO_2 and Cord contents. Additionally, due to the previously described factors, the compressive strength of each of the examined samples increased by 2.81, 7.79, 17.74, and 34.32%. Additionally, as ZrO_2 and Cord concentrations are raised, the resistance of the nanocomposites increases because there are fewer charge carriers, which causes the AC conductivity to constantly decrease. As the quantities of ZrO_2 and Cord increased over time, the study materials' in vitro bioactivity also slightly diminished. Thankfully, the porous nature of the samples and the presence of Mg^{2+} ions in Cord's composition prevented the samples' bioactivity behavior from significantly declining. Strong antibacterial effects against *S. epidermidis* bacteria were seen in all examined samples. However, none of the materials under examination had any effect on the development of *E. coli* bacteria. The results show that the developed nanocomposites may be used to repair damaged bone tissues.

Acknowledgments: This research work was funded by Institutional Fund Projects under grant no. (IFPIP-85-135-1443). The authors gratefully acknowledge the technical and financial support provided by the Ministry of Education and King Abdulaziz University, DSR, Jeddah, Saudi Arabia.

Funding information: This research work was funded by Institutional Fund Projects under grant no. (IFPIP-85-135-1443). The authors gratefully acknowledge the technical and financial support provided by the Ministry of Education and King Abdulaziz University, DSR, Jeddah, Saudi Arabia.

Author contributions: All authors have accepted responsibility for the entire content of this manuscript and approved its submission.

Conflict of interest: The authors state no conflict of interest.

Ethical approval: The research related to human use has been complied with all the relevant national regulations, institutional policies and in accordance the tenets of the Helsinki Declaration, and has been approved by the authors' institutional review board or equivalent committee.

References

[1] Youness RA, TagEl-deen DM, Taha MA. A review on calcium silicate ceramics: properties, limitations, and solutions for their use in biomedical applications. Silicon. 2022, In Press.

[2] Abushanab WS, Moustafa EB, Youness RA. Evaluation of the dynamic behavior, elastic properties, and *In vitro* bioactivity of some borophosphosilicate glasses for orthopedic applications. J Non-Cryst Solids. 2022;586:121539.

[3] Youness RA, Amer MS, Taha MA. Comprehensive in vivo and *In vitro* studies for evaluating the bone-bonding ability of $Na_2O–CaO–SiO_2–B_2O_3–Ag_2O$ glasses for fracture healing applications. Inorg Organomet Polym Mater. 2023, In Press.

[4] Vafa E, Tayebi L, Abbasi M, Azizli MJ, Lari RB, Talaiekhozani A, et al. A better roadmap for designing novel bioactive glasses: effective approaches for the development of innovative revolutionary bioglasses for future biomedical applications. Environ Sci Pollut Res Int. 2022. doi: 10.1007/s11356-022-24176-1.

[5] Vafa E, Lari RB, Bahrololoom ME, Amani AM. Effect of polyvinyl alcohol concentration on biomedical application of chitosan/bioactive glass composite coated on AZ91D magnesium alloy. Mater Chem Phys. 2022;291:126650.

[6] Zhao T, Li. Y, Liu Y, Zhao X. Nano-hardness, wear resistance and pseudoelasticity of hafnium implanted NiTi shape memory alloy. J Mech Behav Biomed Mater. 2012;13:174–84.

[7] Youness RA, Zawrah MF, Taha MA. Synthesis of ZnO-containing calcium silicate nano powders: a study on sinterability, mechanical and electrical properties. Silicon. 2023, In Press.

[8] Bagerifard A, Yekta HJ, Aghdam HA, Motififard M, Sanatizadeh E, Nejad MG, et al. Improvement in osseointegration of tricalcium phosphate-zircon for orthopedic applications: an in vitro and in vivo evaluation. Med Biol Eng Comput. 2020;58:1681–93.

[9] Alturki AM, Abulyazied DE, Taha MA, Abomostafa HM, Youness RA. A study to evaluate the bioactivity behavior and electrical properties of hydroxyapatite/Ag2O-borosilicate glass nanocomposites for biomedical applications. J Inorg Organomet Polym Mater. 2022;32:169–79.

[10] Youness RA, Amer MS, Taha MA. Tribo-mechanical measurements and in vivo performance of zirconia-containing biphasic calcium phosphate material implanted in a rat model for bone replacement applications. Mater Chem Phys. 2022;285:126085.

[11] Youness RA, Ibrahim MA, Taha MA. Evaluation of the electrical and dielectric behavior of the apatite layer on the surface of hydroxyapatite/hardystonite/copper oxide hybrid nanocomposites for bone repair applications. Ceram Int. 2022;48:19837–50.

[12] Heidari F, Tabatabaei FS, Razavi M, Lari RB, Tavangar M, Romanos GE, et al. 3D construct of hydroxyapatite/zinc oxide/palladium nanocomposite scaffold for bone tissue engineering. J Mater Sci Mater Med. 2020;31:85.

[13] Heidari F, Lari RB, Razavi M, Fahimipour F, Vashaee D, Tayebi L. Nano-hydroxyapatite and nano-hydroxyapatite/zinc oxide scaffold for bone tissue engineering application. Int J Appl Ceram Technol. 2020;17:2752–61.

[14] Srivastava A, Singh VK, Kumar V, Kumar PH. Low cement castable based on auto combustion processed high alumina cement and mechanochemically synthesized cordierite: formulation and properties. Ceram Int. 2014;40:14061–72.
[15] Mahdi OS. Preparation cordierite and zirconia-doped cordierite composite and study bioactive properties. Mater Today Proc. 2021;42:2006–11.
[16] Youness RA, Taha MA, Ibrahim MA. The influence of various zirconia contents on crystallite sizes, shrinkage, and physical and mechanical properties of hydroxyapatite-based nanobiocomposites. Egypt J Chem. 2021;64:1347–52.
[17] Jasemi A, Moghadas BK, Khandan A, Samandari SS. A porous calcium-zirconia scaffolds composed of magnetic nanoparticles for bone cancer treatment: Fabrication, characterization and FEM analysis. Ceram Int. 2022;48(1):1314–25.
[18] Youness RA, Taha MA, Ibrahim MA. *In vitro* bioactivity, molecular structure and mechanical properties of zirconia-carbonated hydroxyapatite nanobiocomposites sintered at different temperatures. Mater Chem Phys. 2020;239:122011.
[19] Siswomihardjo W, Sunaritya S, Totowi AE. The effect of zirconia in hydroxyapatite on Staphylococcus epidermidis growth. Int J Biomater. 2012;2012:432372.
[20] Sung YM, Shin YK, Ryu JJ. Preparation of hydroxyapatite/zirconia bioceramic nanocomposites for orthopaedic and dental prosthesis applications. Nanotechnology. 2007;18:065602.
[21] Sivaperumal VR, Mani R, Polisetti V, Aruchamy K, Oh T. Synthesis of hydroxyapatite (HAp)-zirconia nanocomposite powder and evaluation of its biocompatibility: an *In vitro* study. Appl Sci. 2022;12:11056.
[22] Cao Y, Shi T, Jiao C, Liang H, Chen R, Tian Z, et al. Fabrication and properties of zirconia/hydroxyapatite composite scaffold based on digital light processing. Ceram Int. 2020;46:2300–8.
[23] Salehi S, Fathi MH. Fabrication and characterization of sol–gel derived hydroxyapatite/zirconia composite nanopowders with various yttria contents. Ceram Int. 2010;36:1659–67.
[24] Youness RA, Taha MA, Elhaes H, Ibrahim M. Molecular modeling, FTIR spectral characterization and mechanical properties of carbonated-hydroxyapatite prepared by mechanochemical synthesis. Mater Chem Phys. 2017;190:209–18.
[25] Youness RA, Taha MA, Elhaes H, Ibrahim M. Preparation, FTIR characterization and mechanical properties of hydroxyapatite nanopowders. J Comput Theor Nanosci. 2017;14:2409–15.
[26] Kokubo T, Takadama H. How useful is SBF in predicting in vivo bone bioactivity. Biomaterials. 2006;27:2907–15.
[27] Kokubo T, Kushitani H, Sakka S, Kitsugi T, Yamamuro T. Solutions able to reproduce in vivo surface-structure changes in bioactive glass-ceramics A-W. J Biomed Mater Res A. 1990;24:721–34.
[28] Siqueira RL, Zanotto ED. The influence of phosphorus precursors on the synthesis and bioactivity of SiO2-CaO-P2O5 sol-gel glasses and glass-ceramics. J Mater Sci Mater Med. 2013;24:365–79.
[29] Issa SAM, Almutairi AM, Albalawi K, Dakhilallah OK, Zakaly HMH, Ene A, et al. Production of hybrid nanocomposites based on iron waste reinforced with niobium carbide/granite nanoparticles with outstanding strength and wear resistance for use in industrial applications. Nanomaterials. 2023;13:537.
[30] Moustafa EB, Ghandourah E, Youness RA, Melaibari AA, Taha MA. Ultralight functionally graded hybrid nanocomposites based on yttrium and silica-reinforced Mg10Li5Al alloy: thermal and tribomechanical properties. Materials. 2022;15:9052.
[31] Khalil EMA, Youness RA, Amer MS, Taha MA. Mechanical properties, *In vitro* and in vivo bioactivity assessment of Na2O-CaO-P2O5-B2O3-SiO2 glass-ceramics. Ceram Int. 2018;44:7867–76.
[32] Eslami H, Hashjin MS, Tahriri M. Synthesis and charcterization of hydroxyapatite nanocrystals via chemical precipitation technique. Iran J Pharm Sci. 2008;4:127–34.
[33] Fakhruddin AK, Anjalani NA, Mohamad H. Fabrication of bioactive glass-cordierite composite scaffold by gelcasting method. AIP Conf Proc. 2020;2267:020018.
[34] Gheisari H, Karamian E, Abdellahi M. A novel hydroxyapatite–hardystonite nanocomposite ceramic. Ceram Int. 2015;41:5967–75.
[35] Youness RA, Taha. MA, Ibrahim M. In vitro bioactivity, physical and mechanical properties of carbonated-fluoroapatite during mechanochemical synthesis Ceram Int. 2018;44:21323–9.
[36] Lyutova E, Borilo L, Izosimova E. The effect of sodium and magnesium ions on the properties of calcium–phosphate biomaterials. Prog Biomater. 2019;8:127–36.
[37] Lakshmi R, Velmurugan V, Sasikumar S. Preparation and phase evolution of wollastonite by sol-gel combustion method using sucrose as the fuel. Combust Sci Technol. 2013;185:1777–85.
[38] Basheet MH, Farhan FK, Abed AN, Alobaidi OR. The biomedical investigation of bioceramic cordierite as orthopedic material. Key Eng Mater. 2022;937:69–77.
[39] Taha MA, Youness RA, Ibrahim M. Biocompatability, physico-chemical and mechanical properties of hydroxyapatite-based silicon dioxide nanocomposites for biomedical applications. Ceram Int. 2020;46:23599–610.
[40] Hamvar M, Baksheshi-Rad HR, Omidi M, Ismail AF, Aziz M, Berto F, et al. Biocompatibility and bioactivity of hardystonite-based nanocomposite scaffold for tissue engineering applications. Biomed Eng Express. 2020;6:035011.
[41] Taha MA, Youness RA, Zawrah MF. Phase composition, sinterability and bioactivity of amorphous nano-CaO-SiO2-CuO powder synthesized by sol-gel technique. Ceram Int. 2020;46:24462–71.
[42] Gad MM, Al-Thobity AM, Shahin SY, Alsaqer BT, Ali AA. Inhibitory effect of zirconium oxide nanoparticles on Candida albicans adhesion to repaired polymethyl methacrylate denture bases and interim removable prostheses: a new approach for denture stomatitis prevention. Int J Nanomed. 2017;12:5409–19.
[43] Bhattacharya P, Dey A, Neogi S. An insight into the mechanism of antibacterial activity by magnesium oxide nanoparticles. J Mater Chem B. 2021;9:5329.
[44] Nguyen NY, Grelling N, LeeWetteland C, Rosario R, Liu H. Antimicrobial activities and mechanisms of magnesium oxide nanoparticles (nMgO) against pathogenic bacteria, yeasts, and biofilms. Sci Rep. 2018;8:16260.
[45] He Y, Ingudam S, Reed S, Gehring A, Strobaugh Jr TP, Irwin P. Study on the mechanism of antibacterial action of magnesium oxide nanoparticles against foodborne pathogens. Nanobiotechnol. 2016;14:54.
[46] Prakasam M, Locs J, Salma-Ancane K, Loca D, Largeteau A, Berzina-Cimdina L. Fabrication, properties and applications of dense hydroxyapatite: a review. J Funct Biomater. 2015;6:1099–140.
[47] Abushanab WS, Moustafa EB, Youness RA. Mechanical behavior and tribological properties of hydroxyapatite/hardystonite/zirconia hybrid nanocomposites for orthopedic applications. Appl Phys A. 2023, In Press.
[48] Frost HM. Wolff's Law and bone's structural adaptations to mechanical usage: an overview for clinicians. Angle Orthod. 1994;64:175–88.

[49] Mahabole MP, Bahir MM, Kalyankar NV, Khairnar RS. Effect of incubation in simulated body fluid on dielectric and photoluminescence properties of nano-hydroxyapatite ceramic doped with strontium ions. J Biomed Sci Eng. 2012;5:396–405.
[50] Arul KT, Ramya JR, Kalkura SN. Impact of dopants on the electrical and optical properties of hydroxyapatite. In: Vizureanu P, Botelho CMCF, editors. Biomaterials. IntechOpen; 2020 doi: 10.5772/intechopen.93092.
[51] Gittings JP, Bowen CR, Dent ACE, Turner IG, Baxter FR, Chaudhuri JB. Electrical characterization of hydroxyapatite-based bioceramics. Acta Biomater. 2009;5:743–54.
[52] Kalil SM, Beheri HH, Fattah WIA. Structural and electrical properties of zirconia/hydroxyapatite porous composites. Ceram Int. 2002;28:451–8.
[53] Sundarabharathi L, Ponnamma D, Parangusan H, Chinnaswamy M, AlMaadeed MA. Effect of anions on the structural, morphological and dielectric properties of hydrothermally synthesized hydroxyapatite nanoparticles. Appl Sci. 2020;2:1–11.
[54] Hashim A, Hadi Q. Structural, electrical and optical properties of (biopolymer blend/titanium carbide) nanocomposites for low cost humidity sensors. J Mater Sci Mater Electron. 2018;29:11598–604.
[55] Hashim A, Q.Hadi. Synthesis of novel (polymer blend-ceramics) Nanocomposites: structural, optical and electrical properties for humidity sensors. J Inorg Organomet Polym Mater. 2018;28:1–7.
[56] Ahmed H, Hashim A. Fabrication of PVA/NiO/SiC nanocomposites and studying their dielectric properties for antibacterial applications. Egypt J Chem. 2020;63:805–11.